Ferroelectric-Based Nanocomposites: Toward Multifunctional Materials

Stéphane Mornet,*,† Catherine Elissalde,† Olivier Bidault,‡ François Weill,† Elisabeth Sellier,§ Olivier Nguyen,† and Mario Maglione†

Institut de Chimie de la Matière Condensée de Bordeaux, ICMCB UPR CNRS 9048, Université Bordeaux-1, 87 Avenue du Dr A. Schweitzer, F-33608 Pessac, France, Laboratoire de Physique de l'Université de Bourgogne, Faculté des Sciences Mirande, 9 Avenue Alain Savary, B.P. 47870, 21078 Dijon Cedex, France, and Centre de Ressources en Microscopie Electronique, Université Bordeaux, 351, cours de la Libération, 33405 Talence, France

Received July 18, 2006. Revised Manuscript Received November 27, 2006

Nanoparticle technologies open the routes for nanostructured materials which combine individual physical properties or generate new functions. In the field of ferroelectric materials the development of dense nanocomposites requires breakthroughs in the elaboration step. Here, we propose a flexible process to obtain ferroelectric−magnetic nanostructured materials using the assembly of superparamagnetic nanoparticles around ferroelectric cores. The appropriate shaping and sintering of these nanocomposites called nanoraspberries enables a tuning of the physical properties of the resulting dense composite: coexistence between ferroelectricity, piezoelectricity, and superparamagnetism is clearly evidenced at room temperature. This strategy has been also extended to metallic nanoparticles surrounding ferroelectric cores. Our approach combining nanotechnology and solid-state chemistry opens the way to the building of innovative materials for integration and multifunctionality. These are two key points in multidisciplinary fields of applications such as electronics, telecommunications, optics, biomedical, and environment.

Introduction

To achieve nanocomposites, improved strategies are needed to monitor the material up to the final macroscopic scale.[1] Due to the materials choice flexibility, particles self-assembly is a promising route toward nanocomposite materials synthesis. This has already been successfully used in the preparation of photonic crystals,[2] three-dimensional superlattices of magnetic nanocrystals,[3] magnetic nanocomposites,[4,5] and ferroelectric nanostructures.[6] The potentiality of ferroelectric materials is demonstrated not only by the number of applications (i.e., capacitors, transducers, hydrophones, actuators, optical modulators, pyroelectric sensors, photorefractive materials, and tunable microwave devices) but also by the expertise acquired on structure properties relationships in these materials.[7,8] Ferroelectric materials with perovskite structure are well-known for their versatile properties. By simple modifications as substitutions or dopants, characteristics such as transition temperature, disorder, and conductivity can be tuned to reach the targeted applications.[9−11] Besides, in the field of nanosciences, surfaces and interfaces play a key role in modulating the effective properties of materials.

Combining these two fields, the strategy was to use nanoparticles technology to process ferroelectric/superparamagnetic nanocomposites with extended interfaces between the two components in all directions. To achieve such a goal, $Ba_{0.6}Sr_{0.4}TiO_3$ (BST) and $BaTiO_3$ (BT) ferroelectric grains of average size between 150 and 250 nm have been decorated by 7 nm size maghemite (γ-Fe_2O_3) nanocrystals. The covering of both ferroelectric and superparamagnetic grains with a nanoscale amorphous SiO_2 shell is the key step for shaping the final multifunctional 3D composite.

To evidence the multifunctionality, i.e., occurrence of both magnetic and ferroelectric properties, we propose a multiscale process which includes all the different stages from the nanoscopic scale up to final dense material on a macroscopic scale. The challenge here is to preserve the architecture of the composite. Compared to standard ferroelectric composites, our approach is able to increase and accurately control the density of interfaces between the two components.

* Corresponding author. E-mail: mornet@icmcb-bordeaux.cnrs.fr. Tel.: +33 5 40002692. Fax: +33 5 40002761.
† ICMCB-CNRS, Université Bordeaux.
‡ Université de Bourgogne.
§ CREMEM, Université Bordeaux.

(1) Grosso, D.; Boissière, C.; Smarsly, B.; Brezensinski, T.; Pinna, N.; Albouy, P. N.; Amenitsch, H.; Antonietti, M.; Sanchez, C. *Nat. Mater.* **2004**, *3*, 787−792.
(2) Liz-Marzán, L. M.; Mulvaney, P. *J. Phys. Chem. B* **2003**, *107*, 7312−7326.
(3) Pileni, M. P. *J. Phys. Chem. B* **2001**, *105*, 3358−3371.
(4) Lu, A. H.; Li, W. C.; Kiefer, A.; Schmidt, W.; Bill, E.; Fink, G.; Schüth, F. *J. Am. Chem. Soc.* **2004**, *126*, 8616−8617.
(5) Lu, A. H.; Schmidt, W.; Matoussevitch, N.; Bönnemann, H.; Spliethoff, B.; Tesche, B.; Bill, E.; Kiefer, W.; Schüth, F. *Angew. Chem., Int. Ed.* **2004**, *43*, 4303−4306.
(6) Alexe, M.; Scott, J. F.; Curran, C.; Zakharov, N. D.; Hesse, D.; Pignolet, A. *Appl. Phys. Lett.* **1998**, *73*, 1592−1594.
(7) Bhalla, A. S.; Guo, R.; Roy, R. *Mater. Res. Innovat.* **2000**, *4*, 3−26.
(8) Cohen, R. E. *J. Phys. Chem. Solids* **2000**, *61*, 139−146.
(9) Dawber, M.; Rabe, K. M.; Scott, J. F. *Rev. Mod. Phys.* **2005**, *77*, 1083−1130.
(10) Setter, N.; Waser, R. *Acta Mater.* **2000**, *48*, 151−178.
(11) Chu, M.-W.; Szafraniak, I.; Scholz, R.; Harnagea, C.; Hesse, D.; Alexe, M.; Gösele, U. *Nat. Mater.* **2004**, *3*, 87−90.

10.1021/cm0616735 CCC: $37.00
Published on Web 02/08/2007

Experimental Section

Materials. $BaTiO_3$ (BT) and $Ba_{0.6}Sr_{0.4}TiO_3$ (BST) particles of mean diameter close to 50 nm were purchased from Pi-Kem (Shropshire, England). The size of $Ba_{0.6}Sr_{0.4}TiO_3$ particles was increased from 50 to 150 nm by thermal treatment as previously reported.[12] The size of $BaTiO_3$ was increased from 50 to 250 nm by thermal treatment at 1000 °C for 2 h. Iron(III) chloride hexahydrate (98%+), iron(II) chloride tetrahydrate (99%+), iron(III) nitrate nonahydrate (99%+), citric acid (99.5%), and *N*-(trimethoxysilylpropyl)ethylenediamine (AEAPS) (97%) were purchased from Aldrich. Absolute ethanol (J.T. Baker) and ammonia were used as received. Water was deionized (resistivity higher than 18 MΩ). All other reagents were of analytical grade.

γ-Fe_2O_3 Synthesis. Maghemite-based cationic ferrofluids were prepared by alkaline coprecipitation of iron(II) and iron(III) precursors in aqueous solution as previously described.[13] Briefly, the γ-Fe_2O_3 nanoparticles (mean diameter close to 7.5 nm) were synthesized by alkaline coprecipitation of iron(II) and iron(III) precursors in aqueous solution with an excess of concentrated ammonia hydroxide. Then, the magnetite nanoparticles were oxidized into maghemite with iron(III) nitrate at 80 °C. The cationic maghemite ferrofluid was obtained by peptization of nanoparticles flocculates using nitric acid. The final iron concentration was adjusted to 0.25 mol·L^{-1} (20 g·L^{-1} of maghemite) and pH to 2.5.

γ-Fe_2O_3@SiO_2, BST@SiO_2, and BT@SiO_2 Synthesis. Metal oxide nanoparticles were encapsulated by silica with methods previously reported[14−17] and derived from the so-called Stöber process based on the hydrolysis/condensation of TEOS catalyzed by ammonia in alcoholic media.[18] For the ferroelectric particles, the surface was first activated by acidic treatment using a sonicator bath for 15 min in 10 mL of 1 M HNO_3. After being washed by centrifugation, the particle surfaces were citrated by the addition of 0.01 M solution of citric acid. For maghemite nanoparticles, citric acid solution was directly added to the ferrofluid, resulting in the flocculation of the sol. Flocculated citrated nanoparticles were washed with ultrapure water by magnetic sedimentation using a permanent magnet or by centrifugation for citrated-BST and BT particles. Peptization was obtained by adding 20 μL of ammonia on the pellets. Then, each alkaline sol of citrated particles was poured into a volume of ethanol/water/ammonia solution 75/23.5/1.5 v/v/v %. The reaction volume was fixed to 100 mL for BT and BST and to 800 mL for maghemite. To tune the silica shell thickness, the amount of TEOS to be added was calculated from the initial and final particle size, taking into account the number N_p of particles, by means of the formula $V_{TEOS} = 3.89N_p(D^3 - d^3)$, where V_{TEOS} is directly expressed in mL and D and d are the final and the starting diameters expressed in cm. The 3.89 scaling factor was computed from the molecular weights of SiO_2 formula unit and TEOS, the densities of silica and TEOS (2 and 0.934 g·cm^{-3}, respectively) and assuming that particles are spherical. As an example of γ-Fe_2O_3@SiO_2-2nm synthesis, a typical preparation for 6 mL of citrated ferrofluid, 252 μL of TEOS was added for a 2 nm silica shell thickness. After 3 h of reaction time, 200 mL of water was added to the medium and both ammonia and ethanol were removed by using a rotary evaporator at 60 °C. The resulting γ-Fe_2O_3@SiO_2 sol was then adjusted at pH 5 for the next step.

Surface Modification of BST@SiO_2 and BT@SiO_2 by an Aminosilane Coupling Agent. Surface modification of BST@SiO_2-5nm and BT@SiO_2-5nm particles was carried out by adding *N*-(trimethoxysilylpropyl)ethylenediamine (AEAPS, Aldrich, 97%) to the reactive medium at the end of TEOS condensation. Assuming that the surface coverage of AEAPS is nominally 55 $Å^2$/molecule, an excess of 10 equiv of AEAPS, sufficient to provide 2−3 monolayer coatings of the silica nanoparticles, was added. After overnight mixing at room temperature, 100 mL of water was added and both ammonia and ethanol were evaporated at low boil (80 °C) in vacuum. The reaction was followed by a thermal treatment in vacuum at 100−110 °C until the destabilization of the sol (2 h). This operation contributes to the improvement of covalent bonding of the polysiloxane oligomers on to the silica surface. The aminated particles were then washed by centrifugation with water and peptized by addition of 0.1 M chlorhydric acid in the solution until pH 3.5.

Ferroelectric/Magnetic Raspberries Synthesis. The general method used to prepare ferroelectric/magnetic raspberry nanoprecursors for nanocomposites synthesis can be summarized in the following way: BST or BT@SiO_2/Fe_2O_3@SiO_2 nanoraspberries are prepared by slowly adding 40 mL of aminosilane-modified BST or BT@SiO_2 particles (at 8.64×10^{14} and 4.62×10^{12} particles·L^{-1}, respectively, pH 3.5) in to 150 mL of Fe_2O_3@SiO_2 sol (1.83×10^{17} particles·L^{-1}, pH 5). After overnight incubation, the excess of Fe_2O_3@SiO_2 particles was removed by three cycles of centrifugation against ultrapure water. The pellet was dispersed once again in a minimum volume of ultrapure water (1 mL). The resulting heterostructures were deposited onto carbon-coated copper TEM grids for analysis. TEM images were recorded using a Philips EM 120 electron microscope operating at 120 kV.

Ferroelectric/Magnetic Nanocomposites Shaping. The second step of ferroelectric/magnetic nanocomposites synthesis is the sintering of the raspberries to dense three-dimensional ordered compacts. First, the raspberry suspension was naturally sedimented to favor 3D periodic close packing. The aim is to obtain an arrangement closer to 0.63 in the directly obtained green compact (value of the random compact packing fcc structure). Second, an additional decrease of the porosity is obtained by sintering at low temperature. The sintering process consists of a heating treatment in the range 800−900 °C according to the silica thickness embedding the γ-Fe_2O_3 grains (2−5 nm) for 3 h with a preliminary step of 1 h at 680 °C.

Characterizations. Zeta potential of BST and BST@silica nanoparticles were assessed by using a Zetasizer 3000HSA setup (Malvern Instruments) equipped with a He−Ne laser (50 mW, 532 nm). The zeta potential measurement based on laser Doppler interferometry was used to assess the electrophoretic mobility of nanoparticles. Measurements were performed for 20 s using a standard capillary electrophoresis cell. The dielectric constant of solvent (water) was set to 80.4 and the Smoluchowsky constant $f(ka)$ was 1.5.

High-resolution scanning electron microscopy images were collected on a JEOL 6700F. For dielectric and piezoelectric evaluations, the sample was set in a homemade temperature cell and connected to a HP4184 impedance analyzer. The ceramic composites were poled by applying an electric field of 300 kV/cm at a temperature of 450 K and keeping the field during a cooling down to room temperature at a rate of 1 K·min^{-1}. The magnetic

(12) Hornebecq, V.; Huber, C.; Maglione, M.; Antonietti, M.; Elissalde, C. *Adv. Funct. Mater.* **2004**, *14*, 899−904.
(13) Massart, R. *IEEE Trans. Magn.* **1981**, *17*, 1247−1248.
(14) Mornet, S.; Portier, J.; Duguet, E. *J. Magn. Magn. Mater.* **2005**, *293*, 127−134.
(15) Mornet, S.; Elissalde, C.; Hornebecq, V.; Bidault, O.; Duguet, E.; Brisson, A.; Maglione, M. *Chem. Mater.* **2005**, *17*, 4530−4536.
(16) van Ewijk, G. A.; Vroege, G. J.; Philipse, A. P. *J. Magn. Magn. Mater.* **1999**, *201*, 31−33.
(17) Graf, C.; Vossen, D. L.; Imhof, A.; van Blaaderen, A. *Langmuir* **2003**, *19*, 6693−6700.
(18) Stöber, W.; Fink, A.; Bohn, E. *J. Colloid Interface Sci.* **1968**, *26*, 62−69.

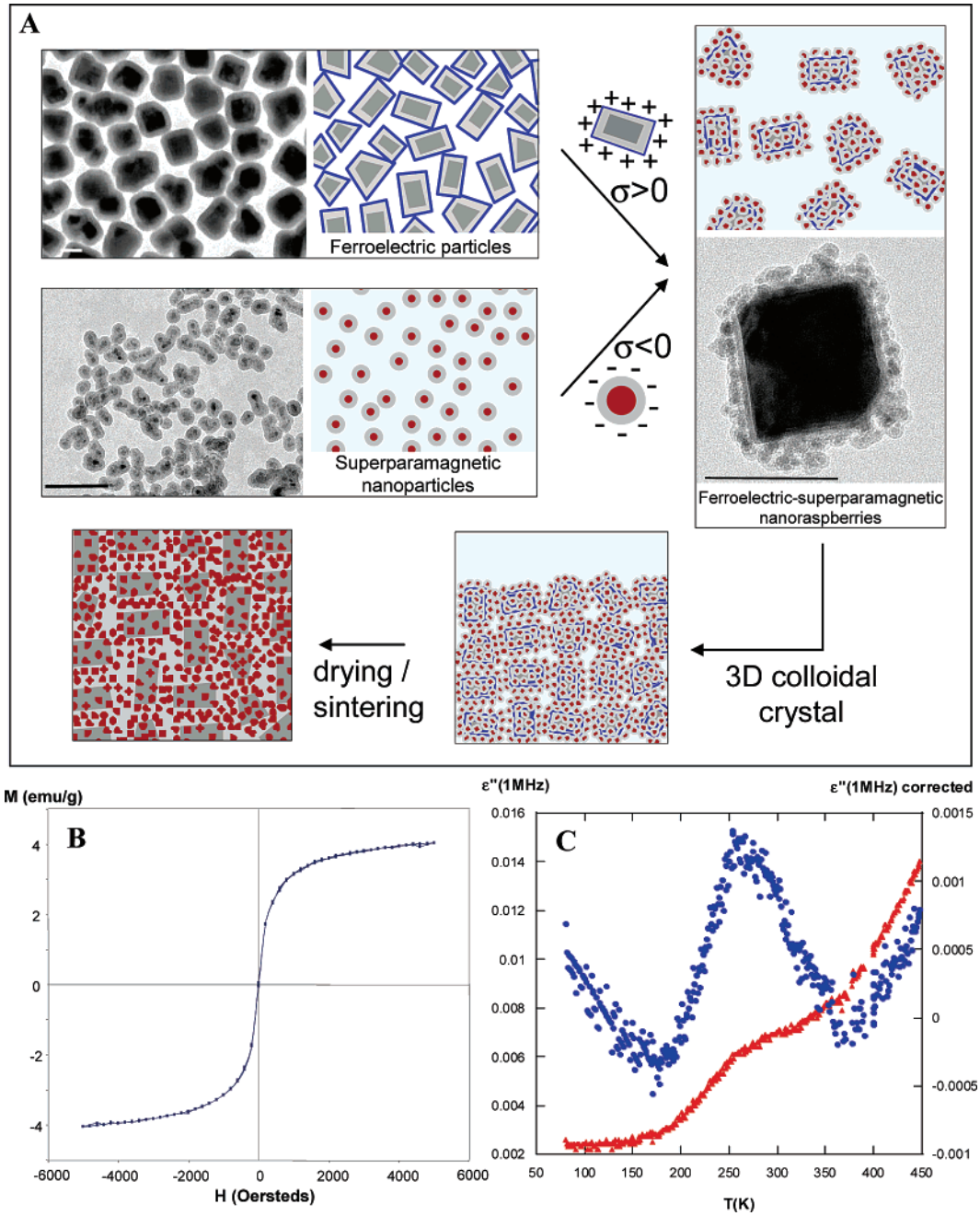

Figure 1. Flow chart of the processing of multifunctional nanostructured materials. (A) The ferroelectric BST@SiO_2 and superparamagnetic γ-Fe_2O_3@SiO_2 crystallites are separately silica-coated and functionalized as to provide oppositely charged particles ($\sigma > 0$ and $\sigma < 0$ respectively where σ is the net surface charge density). Natural electrostatic self-assembly results from this charge imbalance. Due to the good colloidal stability properties of silica, nanoraspberries can self-assembly during the sedimentation step into a colloidal crystal. After drying and sintering a dense nanocomposite is obtained, keeping the raspberry nanoparticles as the individual bricks. During this last step, the thin silica shell favors low-temperature sintering while avoiding grain growth and interdiffusion (scale bar: 100 nm). (B) Field-dependent magnetization recorded at 200 K on sintered colloidal crystal displaying saturation at high fields which calls for superparamagnetism among the γ-Fe_2O_3 nanoparticles; this means that the maghemite cores have not transformed into hematite phase after thermal treatment at 800 °C. (C) Thermal evolution of the imaginary part of the dielectric permittivity (epsilon second). The observed anomaly occurs at the ferroelectric/paraelectric transition temperature of bulk BST. The values of both epsilon second and magnetization at saturation are strongly decreased, by the presence of silica[15] for the first and by the presence of silica[21] and BST for the second.

experiments were performed using a Quantum Design SQUID setup.

Results and Discussion

General Method To Prepare Multifunctional Nanocomposites. The method (Figure 1A) that we have designed is to build brick by brick nanocomposite materials in a bottom-up approach. The first step is the stabilization of the colloids in the reaction medium to encapsulate them by a controlled ultrathin silica layer. The surface of the silica core−shell ferroelectric particles is modified by an aminosilane coupling agent to provide a positively charged surface. Due to the negative charge of γ-Fe_2O_3@SiO_2 particles, nanoraspberries are formed during the mixing with the aminated ferroelectric particles by electrostatic assembly. The nanostructure of individual composite grains is made of a crystalline 150 nm BST or 250 nm BT core coated with silica (BST@SiO_2 and BT@SiO_2, respectively) and surrounded by

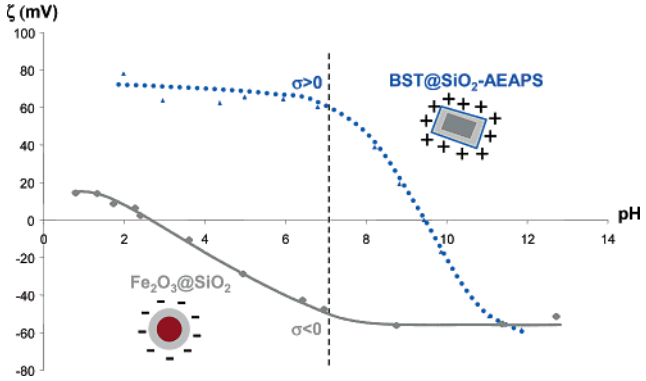

Figure 2. Zeta potential measurements as a function of pH of the aminated BST@SiO_2 particles and the γ-Fe_2O_3@SiO_2 nanoparticles. The best compromise for the strongest electrostatic attractions is toward neutral pH.

7 nm γ-Fe_2O_3@SiO_2 particles. After removal of the excess γ-Fe_2O_3@SiO_2, the nanoraspberries are organized into a three-dimensional colloidal crystal. This procedure, largely used in the field of photonic band gap materials,[2] improves the final composite nanostructure.

Zeta potential measurements have been carried out to obtain the best pH conditions for better electrostatic interactions between the aminated BST(or BT)@SiO_2 particles and the γ-Fe_2O_3@SiO_2 nanoparticles while preserving the stability of the respective colloidal dispersions. The zeta potential curves (Figure 2) of γ-Fe_2O_3@SiO_2 nanoparticles displayed an isoelectric point (IEP) at pH 2.6, in agreement with previous reports (IEPs of silica are equal of 2−3).[19] A single isoelectric point, equal to 2.4 and corresponding to that of silica, has been previously obtained for BST@SiO_2.[15] After silanization of the BST(or BT)@SiO_2 surfaces, the IEP of aminated nanoparticles reached a pH value of 9.5 that corresponds to the pK_a of the primary aminopropyl group. This result indicated a high density of amino groups exposed to the modified-nanoparticle surface. The presence of these protonable amino groups in neutral pH conditions ensures at the same time the electrostatic colloidal stability of these particles and the attractive interactions with the γ-Fe_2O_3@SiO_2 particles. According to the profiles of the two zeta potential curves, the most intense electrostatic interactions are obtained for a pH ranging between 6.5 and 7.5.

In the proposed method, the silica coating is a key parameter not only for (i) the synthesis but also during (ii) the shaping/sintering step and (iii) in the improvement of the final properties: (i) Silica is chosen to stabilize ferroelectric colloidal sols. It is used also as the sticking agent between the two metal oxide phases as to self-assemble them into colloidal crystals. (ii) Silica promotes the chemical stabilization of the components during the densification process in avoiding interdiffusion and, in addition, prevents particles from coalescence. This is a critical point in the case of the γ-Fe_2O_3 nanoparticles which usually transform into hematite (α-Fe_2O_3) at 400 °C with as a result the loss of the superparamagnetic properties. The encapsulation of the maghemite core by silica shifts the structural transition temperature up to 1000 °C according to the silica shell thickness.[20,21] A size effect is believed to be at the origin of this change. In situ X-ray diffraction studies on the α/γ-Fe_2O_3 transition have shown the influence of the surface stress on the nanosized structure stabilization.[22] Cationic diffusion and then coalescence between particles leads to a modification of the surface stress. When the size becomes higher than 20 nm, the hematite phase appears. In addition, the self-assembly properties of the silica core@shell particles are used to suppress the compaction step and to favor the neck formation during the densification step by increasing the solid−solid interfaces density. As a result, sintering occurs at low temperature and then the final grain growth can be prevented, preserving thus the initial raspberry architecture. The sintering is governed by the silica shell and the mechanism for amorphous materials is viscous flow.[23] Previous studies on the sintering of nanometer-sized silica particles revealed a starting temperature for the neck formation as low as 800 °C.[24] (iii) The silica coating precludes conductivity percolation among the superparamagnetic nanoparticles and plays the role of a dielectric barrier between the ferroelectric particles. In addition, the silica coating of the superparamagnetic nanoparticles is believed to affect the contributions of the surface anisotropy and interparticle interactions.[25−28] As a result, changing the silica thickness could lead to dipolar magnetic interaction modifications.

To prevent a dramatic decrease in the capacitance of the final composite, the smallest amount of silica is requested around the ferroelectric particles. At the same time, all the grains must be protected and isolated. Besides, minimal but sufficient silica thickness is required around the magnetic particles to sustain the thermal treatment required for densification without the loss of superparamagnetic properties. A compromise between the contributions mentioned above is necessary to select both the amount of silica coated on each component and the conditions of the thermal densification step. The selected procedure is detailed in the Experimental Section. The SEM observations confirm that the 3D raspberry design is preserved after densification. Sufficient consolidation is obtained to test the dielectric and magnetic properties of the final composite.

Description of the Multifunctionality. The magnetization curve measured at 200 K is analogous to the loops which can be recorded at this temperature on an assembly of maghemite particles, thus showing that the magnetic properties of these grains are kept in the 3D composite (Figure 1B). On Figure 1C, the imaginary part of the dielectric permittivity shows a maximum at the BST transition tem-

(19) Iler, R. K. *The chemistry of silica*; Wiley: New York, 1979; p 98.
(20) Chanéac, C.; Tronc, E.; Jolivet, J. P. *J. Mater. Chem.* **1996**, *6*, 1905−1911.
(21) Mornet, S.; Grasset, F.; Portier, J.; Duguet, E. *Eur. Cells Mater.* **2002**, *3*, 110−113.
(22) Belin, T. Ph.D. Thesis, University of Dijon, France, 2002 (unpublished).
(23) Jagota, A. *J. Am. Ceram. Soc.* **1994**, *77*, 2237−2239.
(24) Miguez, H.; Meseger, F.; Lopez, C.; Blanco, A.; Moya, J. S.; Requena, J.; Misfud, A.; Fornés, V. *Adv. Mater.* **1998**, *10*, 480−483.
(25) Dormann, J. L.; Fiorani, D.; Tronc, E. *J. Magn. Magn. Mater.* **1999**, *202*, 251−267.
(26) Grasset, F.; Labhsetwar, N.; Li, D.; Park, D. C.; Saito, N.; Haneda, H.; Cador, O.; Roisnel, T.; Mornet, S.; Duguet, E.; Portier, J.; Etourneau, J. *Langmuir* **2002**, *18*, 8209−8216.
(27) Vestal, C. R.; Zhang, Z. J. *Nano Lett.* **2003**, *3*, 1739−1743.
(28) Chanéac, C.; Tronc, E.; Jolivet, J. P. *J. Mater. Chem.* **1996**, *6*, 1905−1911.

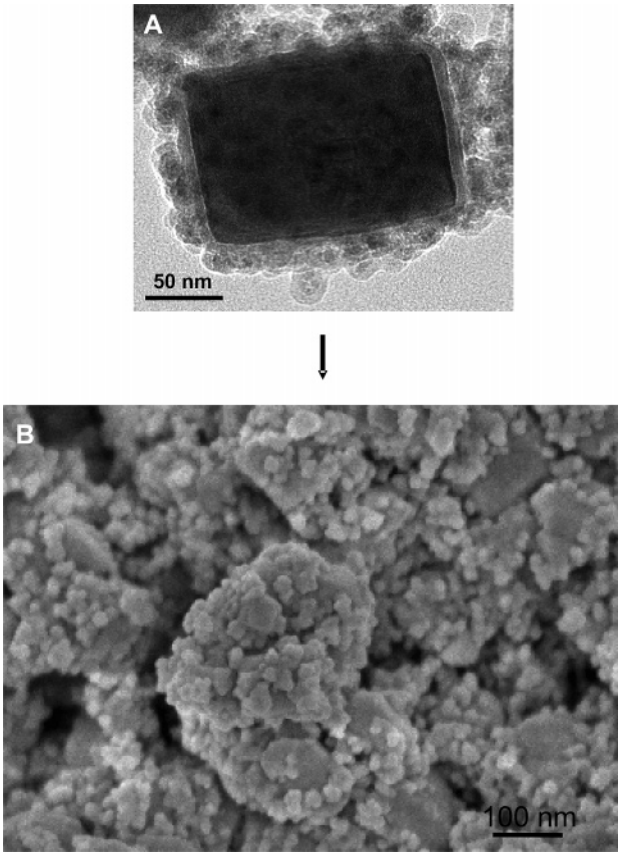

Figure 3. TEM (A) and SEM (B) pictures of respectively (A) raspberry nanoparticle made of ferroelectric $BaTiO_3$@SiO_2 core surrounded by superparamagnetic γ-Fe_2O_3@SiO_2 nanocrystals and (B) raspberries sintered at 800 °C. The raspberry nanodesign is clearly preserved in the bulk samples. The covering of the ferroelectric cores by the superparamagnetic γ-Fe_2O_3 particles is kept in the final ceramic material. Neck formation occurs in the early stage of sintering through viscous flow process due to the silica phase surrounding both ferro and magnetic cores.

perature, which is about 270 K. This is the proof that the intrinsic ferroelectric grains properties are not modified. These results show that ferroelectricity and superparamagnetism do coexist in our raspberry nanocomposite.

A TEM picture of a composite made of cores of $BaTiO_3$ with a different grain size (250 nm) as compared to that of BST is given in Figure 3A. Whatever the morphology and the size of the grain, the silica coating is perfectly controlled. Dielectric permittivity can be tuned in controlling not only the silica thickness but also the ferroelectric core size.[29−32] The sintering process leaves unchanged the raspberry design. A SEM image of the sintered ceramic clearly evidences both the superparamagnetic γ-Fe_2O_3@SiO_2 nanoparticles surrounding the ferroelectric ones (Figure 2B). Although very small because of the SiO_2 shell, the dielectric permittivity of the composite undergoes a clear maximum at the expected transition temperature of $BaTiO_3$ (400 K). We thus found that the nanocomposites do display dielectric anomaly at the expected cores transition temperature for both $BaTiO_3$ and BST. To be conclusive, we further need to probe their electric polarization state. As evidenced in the recent literature,[33] performing ferroelectric hysteresis loops experiments is not an easy task because these require high electric fields and all free charges can lead to spurious loops.

As an alternative route, we performed here piezoelectric resonance experiments which are small signal processes and which are not disturbed by the conductivity. To this aim, the ceramic composites were poled under an electric field. Such a poling was efficient thanks to the outer silica shell which is surrounding the whole ferroelectric/magnetic raspberries. Without such a dielectric barrier, conductivity percolation among the magnetic grains would have cancelled the effective electric field acting on the ferroelectric cores. After the poling process, the piezoelectric resonance was recorded on scanning the frequency of an ac signal of 1V pK−pK and measuring the real and imaginary part of the impedance. This was achieved using the same setup as the one used to record the dielectric data (Figure 1c). A piezoelectric resonance was recorded at a frequency of 2.25×10^6 Hz, showing that the poled composites are noncentrosymmetric. This is evidenced by a steplike decrease of the capacitance and a peak in the dielectric losses. Such a resonance frequency is in the expected range of 3×10^6 Hz/mm for a thickness resonance mode of a $BaTiO_3$ dense ceramic. This agreement shows that our composite is sufficiently densified. The composite nature of our samples also implies very small amplitude of the resonance peak, meaning a tiny piezoelectric coupling factor which could even not be computed from impedance plots. We could however confirm that these composites are indeed piezoelectric. The resonance frequency scaled with the sample thickness: a sample 3 times thicker had a resonance frequency at 9.50×10^5 Hz after the same poling treatment. Its strong decrease on increasing the thickness is a further argument in favor of a piezoelectric activity.

The last and conclusive evidence that the composites are piezoelectric follows from the examination of Figure 4. We clearly see that the resonance amplitude decreases when increasing the temperature up to 430 K, i.e., in the paraelectric/nonpiezoelectric state of $BaTiO_3$ (Figure 3A). The thermal evolution of the integral of the resonance curves shows that the piezoelectric activity of the composites disappears at about 405 K which is the transition temperature evidenced from dielectric experiments (Figure 3B). We can thus conclude that the polarized nanocomposites are noncentrosymmetric and that they recover a centrosymmetric state at the ferroelectric−paraelectric transition temperature. This experiment is thus a conclusive probing of the ferroelectricity of our composites. The temperature shift does not follow the expected decrease when the sample is heated probably because of the composite nature of the ceramic which include materials of different dilatation coefficients. It is also influenced by the transition temperature because of the anomalous variation of the acoustic velocities at these transition points.

(29) Uchino, K.; Sadanaga, E.; Hirose, T. *J. Am. Ceram. Soc.* **1989**, *72*, 1555−1558.
(30) Arlt, G.; Hennings, D.; de With, G. *J. Appl. Phys.* **1985**, *58*, 1619−1625.
(31) Zhao, Z.; Buscaglia, V.; Viviani, M.; Buscaglia, M. T.; Mitoseriu, L.; Testino, A.; Nygren, M.; Johnsson, M.; Nanni, P. *Phys. Rev. B* **2004**, *70*, 024107-1−024107-8.
(32) Frey, M. H.; Xu, Z.; Han, P.; Payne, D. A. *Ferroelectrics* **1998**, *337*, 206−207.
(33) Dawber, M.; Rabe, K. M.; Scott, J. F. *Rev. Mod. Phys.* **2005**, *77* (4), 1063−1130.

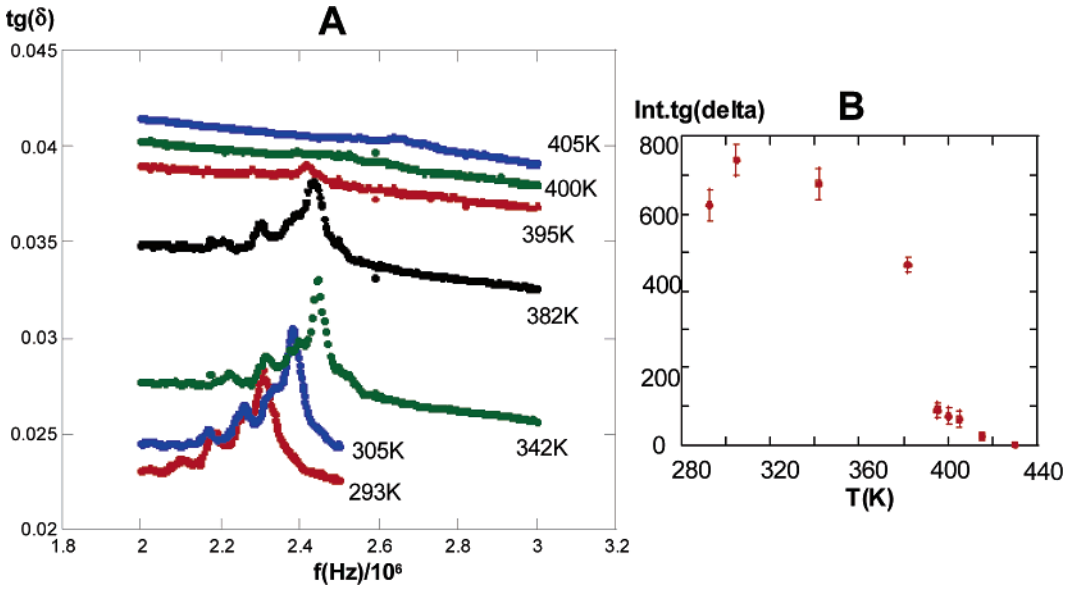

Figure 4. Piezoelectric activity of sintered nanoraspberries. (A) Thermal evolution of the resonance amplitude versus frequency and (B) integral of the resonance curves as a function of temperature. The piezoelectric resonance is a signature of the ferroelectric state of the composite which disappears when the sample transforms into a paraelectric phase at about 400 K, the ferroelectric transition of bulk $BaTiO_3$. We have compared pellets of different size in order to show that the composite resonance frequency does scale with the thickness of the resonator.

This piezoelectric activity of the ferroelectric/magnetic nanocomposites is of strong importance for the search of possible magneto-dielectric coupling properties. Indeed, the direct modulation of a polarization by an external magnetic field needs additional interaction parameters. Several reports and reviews have shown that the elastic deformation can be this additional parameter.[34−39] Piezoelectricity is a useful way to induce such an elastic coupling because of the strong deformation resulting from the applied ac voltage. For example, magneto-electric coupling was evidenced in piezoelectric/ferroelectric laminates made of several thick layers[37] or in simple piezoelectric resonators.[40] The new composites that we have designed include a high density of interfaces between the ferroelectric and the magnetic components of the composite. Strong coupling is thus expected provided the size of the protecting silica shell is kept as low as possible. A magneto-electric coupling would be possible by changing the nature and the size of the ferroelectric cores while keeping the superparamagnetic properties of the raspberry's drupelets.

Conclusion

In summary, here we have demonstrated that, by a simple and flexible process based on a multiscale approach, multifunctional nanostructured materials are provided. The brick by brick design coupled to appropriate shaping/sintering has allowed obtaining original ferroelectric−magnetic 3D composites, built using a raspberry architecture based on silica-coated nanocrystals. Improved multifunctional 3D nanocomposites as compared to standard routes were thus obtained, mainly thanks to extended interfaces between the superparamagnetic nanoparticles and the ferroelectric cores. Multifunctionnality was evidenced in bulk materials by the coexistence at room temperature of magnetic, ferroelectric, and piezoelectric properties in the same composite. This was achieved thanks to the silica shell which not only stabilized the composites but also isolated the different components for example during the poling process. Such coexistence opens the way for improved multifunctional devices and integrated functions in electronic devices. Even if direct coupling between the ferroelectric and magnetic components was not achieved, the coexistence of the two properties and the extreme mechanical distortions at the piezoelectric resonance could be useful to achieve such a coupling. In this way, improved magnetic particles like cobalt-based spinels will be used shortly. Up to now, magneto-dielectric coupling at room temperature was reported in multilayers and integrated nanocomposites. The present report shows that well-organized 3D nanocomposites can be proposed as alternative materials.

Our original approach combining nanotechnology and solid-state chemistry methods opens the way to the building of innovative materials for integration and multifunctionality. These are two key points in multidisciplinary fields of applications such as electronics, telecommunications, optics, biomedical, and environment.

CM0616735

(34) Fiebig, M.; Lottermöser, Th.; Fröhlich, D.; Goltsev, A. V.; Pisarev, R. V. *Nature* **2002**, *419*, 818−820. Fiebig, M. J. *Phys. D: Appl. Phys.* **2005**, *38*, R123−R152.
(35) Kimura, T.; Goto, T.; Shintani, H.; Ishizaka, K.; Arima, T.; Tokura, Y. *Nature* **2003**, *426*, 55−58.
(36) Spaldin, N. A.; Fiebig, M. *Science* **2005**, *309*, 391−392.
(37) Srinivasan, G.; De Vreugd, C. P.; Laletin, V. M.; Paddubnaya, N.; Bichurin, M. I.; Petrov, V. M.; Filippov, D. A. *Phys. Rev. B* **2005**, *71*, 184423-1−184423-6.
(38) Zheng, H.; Wang, J.; Lofland, S. E.; Ma, Z.; Mohaddes-Ardabilli, L.; Zhao, T.; Salamanca-Riba, L.; Shinde, S. R.; Ogale, S. B.; Bai, F.; Vielhand, D.; Jia, Y.; Schlom, D. G.; Wuttig, M.; Roytburd, A.; Ramesh, R. *Science* **2004**, *303*, 661−663.
(39) Eerenstein, W.; Mathur, N. D.; Scott, J. F. *Nature* **2006**, *442*, 759−765.
(40) Maglione, M.; Zhu, W.; Wang, Z. H. *Appl. Phys. Lett.* **2005**, *87*, 092904-1 to 3.